

Disentangled Latent Dynamics Manifold Fusion for Solving Parameterized PDEs

Zhangyong Liang^a, Ji Zhang^{b,*}

^a*National Center for Applied Mathematics, Tianjin University, Tianjin, 300072, PR China*

^b*School of Mathematics, Physics and Computing, University of Southern Queensland, Toowoomba, Queensland, 4350, Australia*

Abstract

Generalizing neural surrogate models across varying partial differential equation (PDE) parameters is a crucial objective in scientific machine learning. However, variations in PDE coefficients frequently alter physical stiffness and spectral complexity, inducing severe optimization failure modes. Furthermore, extending these models to perform reliable temporal extrapolation beyond the training horizon fundamentally exacerbates these challenges. Existing approaches struggle to address both parameter generalization and temporal extrapolation simultaneously. Standard parameterized networks treat time statically, lacking intrinsic dynamical representations. Conversely, recent continuous-time latent models rely on computationally expensive, instance-wise iterative auto-decoding that disrupts the continuous geometry of the parameterized solution space. To address these limitations, we propose Disentangled Latent Dynamics Manifold Fusion (DLDMF), a novel physics-informed framework based on a principled space-time-parameter disentanglement strategy. Rather than relying on unstable test-time auto-decoding, DLDMF explicitly encodes PDE parameters into a continuous latent representation via a deterministic feed-forward mapping. This parameter embedding directly initializes and conditions a continuous temporal latent state, intrinsically governed by a parameter-conditioned neural ordinary differential equation (Neural ODE). Additionally, we introduce a dynamic manifold fusion mechanism. Treating a shared continuous decoder as a manifold

*corresponding author

Email address: `ji.zhang@unisq.edu.au` (Ji Zhang)

network, DLDMF integrates disentangled spatial coordinates, parameter embeddings, and time-evolving latent dynamical states. This architecture thus decodes these intrinsic latent trajectories into physically consistent, parameterized spatiotemporal solutions in the physical domain. By shifting temporal prediction from static coordinate regression to intrinsic dynamic flow integration, our formulation structurally decouples parameter-induced stiffness from temporal dynamics. Consequently, DLDMF preserves global geometric coherence, yielding robust predictive accuracy under unseen parameter configurations while performing challenging long-term temporal extrapolation. Extensive experiments on representative benchmarks validate our method, demonstrating that DLDMF significantly outperforms state-of-the-art baselines in predictive accuracy, parameter generalization, and extrapolation robustness.

Keywords: Parameterized partial differential equations, physics-informed neural networks, continuous-time latent dynamics, manifold fusion, temporal extrapolation.

1. Introduction

Scientific machine learning (SML) [3] has witnessed rapid progress in recent years, primarily driven by the increasing demand for efficient and accurate solvers for partial differential equations (PDEs). Compared to classical numerical models—such as finite element, finite volume, or spectral methods [35]—learning-based approaches offer novel opportunities to construct flexible surrogate models capable of leveraging data, reducing computational costs, and operating effectively in high-dimensional settings. Consequently, a prominent line of research has focused on embedding physical laws directly into neural networks. This integration yields physically consistent and structure-preserving models, encompassing conservation-law-constrained methods [42, 28], Hamiltonian and Lagrangian neural networks [20, 51, 34, 11, 29], as well as symmetry-aware architectures [4, 18]. Among these, Physics-Informed Neural Networks (PINNs) [42] have emerged as a widely adopted framework, owing to their simple formulation, seamless compatibility with automatic differentiation [5], and ease of implementation within modern deep learning libraries like PYTORCH [38] and TENSORFLOW [1]. By concurrently minimizing PDE residuals and initial/boundary condition losses, PINNs facilitate the resolution of PDEs even without exact paired data. As a result,

they have demonstrated considerable success across diverse applications, notably in fluid dynamics [46, 22, 23].

Regardless of their flexibility, standard PINNs are typically trained for a single configuration of PDE parameters, boundary conditions, and geometries, fundamentally limiting their applicability in parametric settings. To address this limitation, recent work has explored parameter-generalized models targeted at solving entire families of PDEs within a unified framework. Representative strategies include hypernetwork-based PINNs [32], meta-learning approaches such as auto-decoding [36] and meta-auto-decoding (MAD) [21], along with operator-learning methods that directly map parameterized inputs to solution spaces [31, 33]. Within this evolving landscape, Parameterized Physics-Informed Neural Networks (P²INNs) [10] offer a particularly appealing formulation. By explicitly encoding PDE parameters into a latent representation, they utilize this embedding to parameterize the underlying solution network. Rather than merely treating PDE parameters as additional input coordinates, P²INNs construct a dedicated parameterized solution manifold. This architectural choice enables a single model to adapt to novel parameter configurations without requiring retraining from scratch. Notably, such a latent manifold perspective has been shown to substantially enhance both robustness and predictive accuracy, especially for highly non-linear PDEs across challenging parameter regimes.

However, while P²INNs effectively address parameter generalization, they inherit a fundamental drawback shared by most coordinate-based PINN architectures: the absence of intrinsic temporal modeling. In standard P²INNs, time is purely treated as an additional static coordinate, and the solution network is optimized over a fixed temporal window. Consequently, the learned representation lacks the structure of an underlying dynamical system, causing extrapolation capabilities beyond the training horizon to deteriorate rapidly. This limitation proves particularly restrictive for long-term forecasting and dynamical analysis tasks, where accurately capturing continuous temporal evolution is just as critical as spatial representation and parameter generalization.

To explicitly overcome this absence of intrinsic temporal structure, recent studies have proposed modeling PDE dynamics directly within the latent space. Dynamics-aware implicit neural representations, such as DINO [60], and physics-informed latent dynamics models, like PIDO [52], introduce neural ordinary differential equations (Neural ODEs) [9] to characterize continuous-time evolution within a low-dimensional latent space. By learning an under-

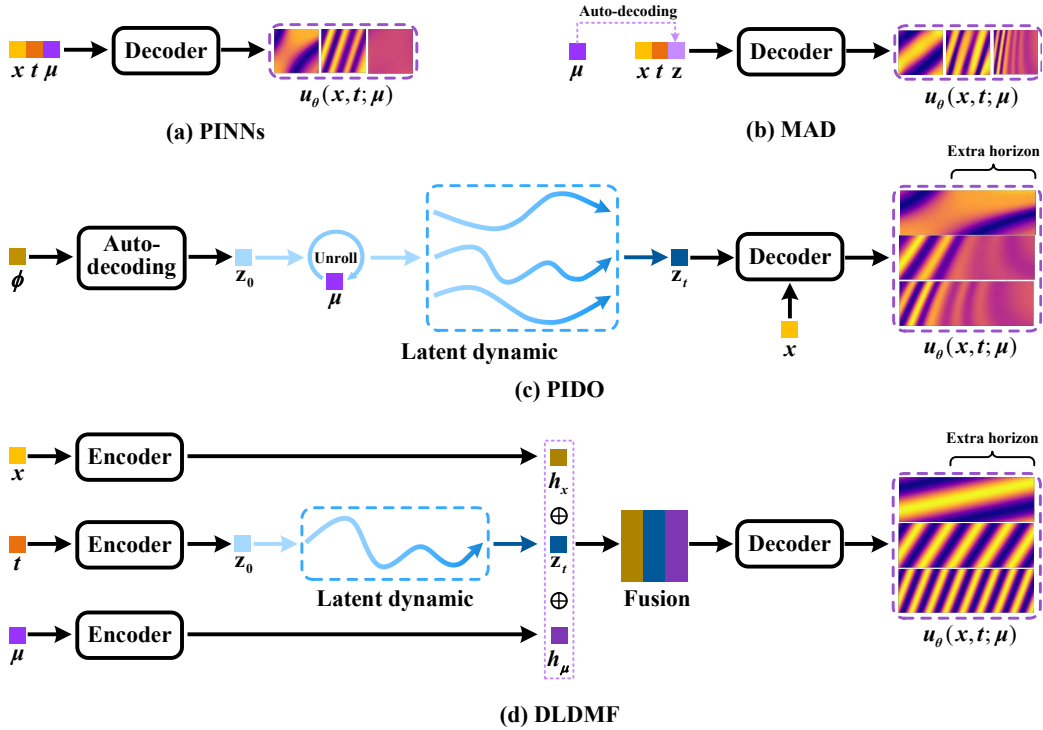


Figure 1: Physics-informed neural PDE solvers. Colorful squares denote spatial (x , yellow), temporal (t , orange), parameter (μ , purple), or initial observation (ϕ , brown) inputs. (a) **PINNs** process concatenated inputs directly through a decoder. (b) **MAD** learns a latent state z for specific parameters via test-time auto-decoding. (c) **PIDO** relies on auto-decoding the initial observations ϕ to obtain a state z_0 , then unrolls latent dynamics conditioned on μ . (d) **DLDMF (ours)** explicitly disentangles representations by passing x , t , and μ through separate feed-forward encoders, completely avoiding iterative auto-decoding. The temporal branch unrolls the latent state z_0 into continuous trajectories z_t via a dynamics model. A dedicated fusion block then integrates spatial (h_x), temporal (z_t), and parameter (h_μ) embeddings before decoding. This design intrinsically supports long-term temporal extrapolation (“Extra horizon”) and enables rapid generalization to varying PDE coefficients.

lying latent flow rather than individually regressing solution values at discrete time points, these methods exhibit robust long-term extrapolation capabilities. Nevertheless, such latent dynamics approaches heavily rely on encoding initial conditions to derive latent states, tailoring them predominantly toward initial-value generalization. Thus, this dependence on initial condition encoding renders them ill-suited for parameterized PDE settings, where the main source of variability stems from the PDE coefficients rather than the initial states themselves.

In this work, we aim to bridge the conceptual gap between parameterized solution manifolds and intrinsic latent dynamics. To this end, we introduce Disentangled Latent Dynamics Manifold Fusion (DLDMF), a versatile physics-informed framework uniquely capable of generalizing across varying PDE coefficients while rigorously extrapolating beyond the training time horizon. The key to the success of DLDMF lies in its disentangled architecture and dynamic manifold fusion mechanism, which fundamentally distinguish it from existing paradigms (as illustrated in Fig. 1). Standard PINNs (Fig. 1a) process time and parameters essentially as static coordinates. Methods like MAD (Fig. 1b) obtain latent codes via test-time auto-decoding, whereas continuous-time models like PIDO (Fig. 1c) rely on auto-decoding initial observations to unroll latent trajectories. In stark contrast, DLDMF (Fig. 1d) explicitly disentangles spatial coordinates, temporal dynamics, and PDE parameters through dedicated feed-forward encoders, thereby completely bypassing the computational bottleneck associated with iterative auto-decoding. Specifically, DLDMF utilizes feed-forward mappings to generate spatial embeddings (h_x), parameter embeddings (h_μ), and an initial temporal latent state (z_0). Modulated by a parameter-conditioned Neural ODE [9], this temporal state continuously evolves into z_t , intrinsically supporting long-term temporal extrapolation. Ultimately, a shared fusion mechanism harmoniously integrates h_x , z_t , and h_μ prior to decoding. This synergistic integration yields physically consistent spatiotemporal solutions while structurally decoupling parameter-induced stiffness from dynamic temporal progression.

Our core contributions are summarized as follows:

- **A Unified Dynamic Framework:** We propose Disentangled Latent Dynamics Manifold Fusion (DLDMF), a novel physics-informed architecture bridging parameterized solution manifolds with intrinsic continuous-time latent dynamics. This integrated approach success-

fully overcomes the fundamental limitations of standard static coordinate-regression in PINNs when solving time-dependent parameterized PDEs.

- **Space–Time–Parameter Disentanglement:** We introduce a principled representation paradigm where PDE coefficients, spatial coordinates, and temporal states are modeled through distinct manifolds. By integrating them via a shared dynamic manifold fusion decoder, our model structurally decouples parameter-induced stiffness from temporal evolution while preserving geometric coherence across the spatial domain.
- **Amortized Feed-Forward Latent Initialization:** Rather than relying on computationally expensive and often unstable test-time iterative auto-decoding, DLDMF adopts a deterministic feed-forward mapping approach. It explicitly encodes PDE parameters to instantaneously initialize a parameter-conditioned Neural ODE, entirely eliminating inverse-problem bottlenecks during inference.
- **Efficient Fine-Tuning via SVD Modulation:** To further enhance solution accuracy for specific downstream deployment scenarios, we implement an SVD-based structural modulation mechanism. By extracting and selectively optimizing singular value bases from the pre-trained manifold network, DLDMF rapidly adapts to targeted PDE configurations with minimal computational overhead.
- **Robust Generalization and Extrapolation:** We thoroughly validate the efficacy of DLDMF through rigorous benchmarks, investigating highly nonlinear Convection–Diffusion–Reaction equations alongside 2D fluid dynamics. The proposed methodology naturally extends to out-of-distribution regimes, demonstrating exceptional parameter generalization and yielding stable, reliable long-term temporal extrapolation that significantly outperforms current state-of-the-art baselines.

2. Related works

Machine learning methods for solving PDEs. Classical numerical solvers for partial differential equations (PDEs)—such as finite difference and finite element methods—offer well-established accuracy guarantees; however, they frequently incur prohibitive computational costs due to dense grid refinement

requirements [39, 30, 49]. To circumvent these limitations, machine learning approaches have gained significant traction as efficient surrogate models for conventional PDE solvers [24]. Early data-driven attempts predominantly featured variational formulations based on the Galerkin or Ritz methods [43]. These were eventually unified under the Physics-Informed Neural Network (PINN) paradigm [42]. Specifically, PINNs parameterize PDE solutions utilizing coordinate-based neural networks, enforcing governing equations via differentiable residual losses [42, 61]. Consequently, this elegant formulation facilitates mesh-free training and inference through automatic differentiation [5], yielding successful applications across diverse domains like fluid dynamics and transport phenomena [46, 22, 23]. Nevertheless, despite their inherent flexibility, PINNs frequently encounter severe optimization landscapes and acute sensitivity to physical stiffness, particularly when solving highly nonlinear or multi-scale PDEs [26, 55].

Physics as inductive biases. Systematically embedding physical principles into neural architectures has been extensively investigated to bolster model generalization and numerical stability [12, 29]. Historically, structural biases have been integrated either through specialized architectural designs—exemplified by Hamiltonian and Lagrangian neural networks [20, 51, 34, 11]—or via rigorously constrained optimization frameworks [43]. Conversely, PINNs adopt a distinctly straightforward yet versatile strategy: directly embedding governing PDE operators along with initial and boundary conditions as soft constraints within the aggregate loss function [42]. Crucially, this physics-informed loss framework bypasses the necessity for perfectly paired ground-truth data. As a result, it has catalyzed a multitude of algorithmic extensions specifically tailored to enhance optimization robustness [57, 54, 59] and accelerate convergence dynamics [26].

Parameterized PDEs learning. A prominent bottleneck of standard PINNs remains their inability to generalize across varying PDE coefficients, divergent initial conditions, or altered geometries without performing computationally prohibitive retraining [32]. To effectively address this issue, operator learning frameworks have emerged, shifting the paradigm towards learning continuous mappings between infinite-dimensional function spaces [31, 33]. For instance, neural operators such as Fourier Neural Operators and DeepONets facilitate parameterized PDE emulation. However, they frequently maintain a rigid dependence on fixed spatial discretizations or require massive datasets of paired solutions [31, 33, 27]. Physics-informed extensions,

including PI-DeepONet, incorporate PDE residual losses to mitigate data requirements; nonetheless, they typically rely on linear conditioning for parameter embeddings, which fundamentally limits representational expressivity [56, 27]. Simultaneously, alternative meta-learning strategies, notably meta-auto-decoding (MAD), directly optimize task-specific latent variables without a dedicated encoder [21]. Returning to the PINN framework, P²INNs dynamically encode continuous PDE parameters into a dedicated latent representation, actively constructing a parameterized solution manifold. This deliberate architectural choice allows a single model to adapt seamlessly to novel parameter configurations [26]. By modeling this continuous manifold rather than merely treating physical coefficients as naive geometric coordinates, such architectures substantially improve overall robustness and predictive fidelity perfectly suited for challenging parameter regimes [26].

Implicit neural representations. Implicit neural representations (INRs) mathematically model continuous signals by utilizing coordinate-based networks to map spatial or spatiotemporal inputs directly to function values [47, 14]. When applied to PDEs, INRs yield essentially grid-agnostic representations properly queryable at arbitrary domain locations [47]. In this view, PINNs can natively be interpreted as physics-informed spatiotemporal INRs. Yet, their standard formulation restricts them strictly to resolving isolated initial-boundary value instances [42]. Subsequent extensions of INRs targeting multi-sequence modeling have introduced latent conditioning variables derived from initial system states, enabling the encapsulation of divergent physical trajectories within a unified architecture [62, 48, 7]. Crucially, however, these approaches predominantly construct static block mappings from initial conditions to solution trajectories spanning a fixed time horizon, neglecting to capture intrinsic dynamical flows [15, 8]. As a consequence, achieving reliable long-term extrapolation beyond the immediate constraints of the training interval remains intensely challenging for traditional INR-based solvers [60].

Latent dynamics modeling. Explicit dynamics modeling (EDM) conceptually refocuses learning objectives toward the continuous time derivatives of evolving system states rather than strictly regressing absolute solution amplitudes [19]. While autoregressive EDM schemes accurately approximate temporal evolution via discrete sequential stepping, they are frequently bounded by fixed step-size constraints and detrimental error accumulation [6]. To

resolve this, neural ordinary differential equations (Neural ODEs) offer a continuous-time workaround by parameterizing the governing vector fields, which can subsequently be integrated across arbitrary temporal landmarks [9]. Accordingly, Neural ODEs possess distinguished temporal extrapolation capabilities well-regarded in continuous-time modeling [40, 2]. Pioneering frameworks like DINO seamlessly leverage these Neural ODEs confined within a reduced latent space, integrating them with INR decoders to characterize complex spatiotemporal dynamics over continuous domains [60]. Similarly, paradigms such as PIDO blend physics-informed optimizations intrinsically with latent trajectory modeling, successfully achieving holistic generalization across varied initial configurations and distinct PDE coefficients [52]. Despite their proven empirical success in extended forecasting, these latent dynamics methodologies universally depend on directly encoding early conditions into the hidden state. This dependency intrinsically limits their adaptability in distinctly parameterized settings, where prevailing dynamics variance is dictated overwhelmingly by operator parameters instead of initial snapshot structures [60, 52]. Furthermore, an overarching limitation persists: multiple EDM-based toolkits enforce strictly data-driven training regimens or impose severely restrictive conditions upon input data grids and distributions [45, 58].

3. Problem formulation

In this section, we formalize the learning setting for time-dependent parameterized PDEs alongside the diverse extrapolation regimes of analytical interest. Subsequently, we critically review the established latent-dynamics modeling pipeline grounded in auto-decoding. By explicitly highlighting its intrinsic constraints, we elucidate precisely why eliminating test-time iterative latent inference constitutes a vital prerequisite for constructing efficient and highly responsive manifold-fusion solvers.

3.1. Parameterized PDEs

We meticulously evaluate families of time-dependent parameterized PDEs formulated over a designated spatial domain $\Omega \subset \mathbb{R}^{d_x}$ across a specified time interval $t \in [0, T]$:

$$\mathcal{F}(x, t, u, \partial_t u, \nabla_x u, \nabla_x^2 u; \boldsymbol{\mu}) = 0, \quad (x, t) \in \Omega \times [0, T], \quad (1)$$

which remain stringently subject to corresponding initial boundary constraints:

$$u(x, 0; \boldsymbol{\mu}) = u_0(x; \boldsymbol{\mu}), \quad \mathcal{B}(x, t, u, \nabla_x u; \boldsymbol{\mu}) = 0, \quad (x, t) \in \partial\Omega \times [0, T], \quad (2)$$

where $u(x, t; \boldsymbol{\mu}) \in \mathbb{R}^{d_u}$ expressly denotes the PDE solution profile, and $\boldsymbol{\mu} \in \mathbb{R}^{d_\mu}$ uniquely encapsulates distinct PDE parameters (e.g., differential operator coefficients). Functionally, physics-informed learning endeavors to mathematically synthesize a continuous neural surrogate function $u_\Theta(x, t; \boldsymbol{\mu})$ that permits queries at entirely arbitrary coordinates (x, t) , uniformly satisfying the requisite governing physics via continuously differentiable residual penalizations—crucially, without enforcing dependence upon perfectly paired trajectory data.

To comprehensively describe the mechanism underlying temporal extrapolation in a manner consistent with latent-dynamics forecasting paradigms, we interpret an individual PDE solution analytically as a trajectory $v : \mathbb{R} \rightarrow \mathcal{V}$ navigating through a defined functional space \mathcal{V} encompassing spatial functions conforming to $\Omega \rightarrow \mathbb{R}^{d_u}$, wherein we formally designate $v_t \triangleq v(t)$. We explicitly concentrate on standard initial value formulation scenarios, prioritizing conditions where uniquely the system state defined at time t proves strictly necessary to robustly infer subsequent emergent states $v_{t'}$ defined for arbitrary $t' > t$. During standard optimization training, observed or mathematically assessed trajectories fundamentally derive from a bounded collection of distinct, strictly discrete time instances $\mathcal{T} \subset [0, T_{\text{tr}}]$ mapped across a generalized, arbitrary spatial grid configuration $\mathcal{X}_{\text{tr}} \subset \Omega$. Conversely, during subsequent out-of-distribution inference testing, it is typically presumed that singularly a novel initialized starting condition v_0 is securely available—frequently sampled upon a distinctively diverse grid structure $\mathcal{X}_{\text{ts}} \subset \Omega$. Resultantly, the actual predictive inference effectively operates across fully arbitrary spatial networks $\mathcal{X}' \subset \Omega$ spanning arbitrary time distributions $\mathcal{T}' \subset [0, T']$; structurally, this projected inference horizon frequently heavily exceeds the foundational trained bounds such that rigorously $T' > T_{\text{tr}}$. For descriptive convenience extending through subsequent discussions, we label spatial evaluations spanning inside and formally outside standard evaluated boundaries distinctly as *In-s* ($x \in \mathcal{X}_{\text{tr}}$) versus *Out-s* ($x \in \mathcal{X}_{\text{ts}}$). Commensurately, temporal queries are logically divided identically between *In-t* representing ($t \leq T_{\text{tr}}$) uniformly distinct from *Out-t* extrapolation cases defining ($t > T_{\text{tr}}$).

Serving fundamentally as our deeply established primary representative empirical benchmark category, we analytically scrutinize the prominent one-dimensional universally parameterized Convection–Diffusion–Reaction (CDR) system equations:

$$\frac{\partial u}{\partial t} + \beta \frac{\partial u}{\partial x} - \nu \frac{\partial^2 u}{\partial x^2} - \rho u(1 - u) = 0, \quad x \in \Omega, t \in [0, T]. \quad (3)$$

wherein precisely β tightly regulates advective convection propagation intensity, ν selectively controls molecular scale diffusion tendencies, while predictably ρ dynamically scales the highly reactive Fisher-type interaction formulation $\rho u(1 - u)$. Consequently, this distinguished family serves pervasively specifically to accurately quantify complex physics-informed meta-learning across drastically contrasting coefficient domains. Specifically, continuous solution profiles vary inherently radically corresponding intimately with divergent (β, ν, ρ) permutations—frequently deliberately encompassing profoundly rigorous sub-regions demonstrably documented universally to severely exacerbate fundamental gradient-descent failure modes uniquely triggered via innate spectral bias combined dynamically alongside underlying numeric stiff constraints. We heavily emphasize directly that resolutely navigating this mathematically parameterized CDR framework systematically remains exhaustively sufficient critically to empirically stress-test essential components encompassing: (i) structural parametric functional generalization spanning highly turbulent coefficient fluctuations, (ii) pure rigorous temporal long-horizon forward extrapolation spanning securely past strict training temporal ceilings, and explicitly subsequently (iii) profound parameter space numeric extrapolation definitively surpassing predefined bounded analytical training distributions. Universally, confronting these combined scenarios cumulatively heavily uncovers inherent learning optimization difficulty fundamentally delineating distinct upper generalization ceiling limitations.

While intrinsically powerful, canonical PINNs remain profoundly constrained by several well-documented structural weaknesses that limit their operational scalability. Primarily, the inherent differential PDE operators typically exhibit acute nonlinearity, rendering the associated mathematical gradient landscapes profoundly unstable and exceptionally challenging to optimize. Furthermore, substantial computational inefficiencies emerge from their repetitive structural formulation: initializing and training a fundamentally distinct model strictly from randomized scratch is consistently demanded whenever exact solutions to newly parameterized PDE variations

are sought. Historically, extensive methodological investigations have systematically attempted to mitigate these discrete constraints. For instance, structured curriculum-learning-inspired algorithmic sequences have been deployed, methodically transitioning initialization states by gradually progressing from empirically “easy” benchmark equations toward significantly more demanding “hard” parametric configurations¹. Simultaneously, alternative architectures have heavily leveraged meta-learning techniques—most notably Meta-PINNs implementations [32]—to effectively establish broadly applicable global solver generalizations mapping $u_{\Theta}(x, t; \boldsymbol{\mu})$, wherein $\boldsymbol{\mu}$ rigidly encapsulates bounded parametric vector distributions like $\boldsymbol{\mu} = [\beta, \nu, \rho]$ characterizing the underlying CDR formulations. Nevertheless, despite these significant architectural advancements, contemporary research has distinctly lacked a rigorously unified mathematical framework capable of simultaneously tackling parameter-driven generalization dependencies whilst unequivocally succeeding in rigorous, long-horizon temporal forward extrapolations extending directly past defining *Out-t* bounds [26, 52, 60].

3.2. Auto-decoding for latent space dynamics

A prominent methodology for achieving reliable long-horizon temporal forecasting involves learning intrinsic latent dynamics within a significantly reduced low-dimensional manifold, subsequently decoding these representations back into a continuous physical spatial field [60, 52]. Specifically, given an observed trajectory sequence $\{v_t\}_{t \in \mathcal{T}}$, a dedicated encoder initially computes corresponding latent formulation states α_t directly from periodic observations as $\alpha_t = E_{\varphi}(v_t)$. Following this encoding, a matching continuous decoder progressively reconstructs the structural space variable v_t governed by $D_{\phi}(\alpha_t)$. Consequently, the continuous latent temporal evolution is structurally modeled leveraging a continuous-time dynamic mathematical framework—typically taking the operational form of a parameterized Neural Ordinary Differential Equation (Neural ODE):

$$\frac{d\alpha_t}{dt} = f_{\psi}(\alpha_t), \quad \alpha_{t+\tau} = \alpha_t + \int_0^{\tau} f_{\psi}(\alpha_{t+s}) ds, \quad (4)$$

enabling arbitrary continuous predictions and robust mathematical extrapolation securely beyond the foundational boundaries of the training horizon

¹Following the notational conventions in curriculum learning, we use the terms, “easy” and “hard,” to indicate data that are easy or hard for neural networks to learn.

via continuous numerical integration.

A paramount computational challenge arises during deployment, however: at inference time, strictly only the initialized starting condition v_0 is typically available. Consequently, the fundamental latent initial state α_0 must necessarily be accurately inferred to appropriately initialize the governing ODE system. Since α_t remains implicitly defined via the inverse mapping $D_\phi(\alpha_t) \approx v_t$, several existing INR-based structural dynamics architectures deliberately navigate this inverse mapping process by incorporating active auto-decoding methodologies in lieu of a standardized feed-forward encoding module [37]. Formally defining the reconstruction decoding loss as $\ell_{\text{dec}}(\phi, \alpha_t; v_t) = \|D_\phi(\alpha_t) - v_t\|_2^2$, auto-decoding fundamentally defines the “encoder” entirely as a constrained iterative numerical optimization procedure:

$$E_\varphi(v_t) = \alpha_t^K, \quad \alpha_t^{k+1} = \alpha_t^k - \eta \nabla_{\alpha_t} \ell_{\text{dec}}(\phi, \alpha_t^k; v_t), \quad k = 0, \dots, K - 1. \quad (5)$$

where precisely α_t^0 designates an initial starting approximation while the designated metric norm anchoring ℓ_{dec} is structurally evaluated uniformly spanning the directly observed coordinate discretization grid. Compared explicitly with standard amortized static auto-encoding, this dynamic auto-decoding technique demonstrably mitigates critical underfitting vulnerabilities while explicitly avoiding imposing inflexible or specialized encoder topology constraints—an especially appealing fundamental attribute specifically applicable across highly irregular, non-uniform observational measurement grids.

Despite exhibiting such conceptual flexibility, widespread auto-decoding architectures intrinsically introduce fundamental algorithmic limitations severely restricting continuous latent space temporal dynamics modeling [21]. Foremost, this architecture strictly requires computationally exhaustive, instance-wise iterative optimization precisely at operational inference time; this structural dependency inevitably incurs exceptionally high processing latency, rendering real-time operational deployment drastically fundamentally challenging. Secondly, when auto-decoding methodologies are extensively leveraged dynamically representing massively diverse parametric instances (e.g., projecting dense solution trajectories across heavily disparate temporal snapshots), the system obligatorily requires perpetually maintaining vastly expansive collections incorporating millions of distinct latent numerical codes and associated transient optimizer matrices, instigating severe scalability and memory allocation bottlenecks. Thirdly, to strictly preserve overall integration tractability governing latent temporal dynamics, existing pipelines

repeatedly structurally depend completely upon preliminary reduced-order modeling (ROM) methodologies or extensively simplified low-dimensional latent approximations strictly before ultimately initiating standard Neural ODE propagation schemes [16, 8, 60]. Considering these profound cumulative deficiencies, these foundational issues unequivocally conceptually motivate deliberately replacing traditional auto-decoding-based transient latent inference methodologies directly with a highly stable, deterministic parameter-explicitly-conditioned structural mechanism reliably capable of autonomously initializing deep latent dynamics uniformly without perpetually requiring demanding iterative test-time numerical optimization.

3.3. Static parameterized solution manifolds

Parameterized PINN architectures effectively address these limitations by learning a single unified model deliberately conditioned upon varying PDE parameters, frequently accomplished by formulating $u_{\Theta}(x, t; \boldsymbol{\mu})$ directly [10]. In particular, P²INN significantly advances this paradigm by articulating a distinct manifold perspective; it rigorously encodes PDE parameters specifically into an overarching hidden representation defined as $h_{\text{param}} = g_{\theta_p}(\boldsymbol{\mu})$, subsequently leveraging this construct to mathematically modulate the structural coordinate-based solver dynamics [26]. A characteristic archetypal formulation is robustly expressed as:

$$h_{\text{coord}} = g_{\theta_c}(x, t), \quad h_{\text{param}} = g_{\theta_p}(\boldsymbol{\mu}), \quad u_{\Theta}(x, t; \boldsymbol{\mu}) = g_{\theta_g}(h_{\text{coord}}, h_{\text{param}}). \quad (6)$$

where exactly g_{θ_g} precisely functions as the defining manifold integration network exclusively harmonizing embedded coordinate values synergistically alongside encoded parameter variables.

Ultimately, this explicitly differs from standard conventional instance-parameterized optimization configurations typified comprehensively by methodologies precisely like MAD, which rigorously introduce an independently floating latent vector rigidly assigned per individual distinct modeling instance, obligatorily co-optimizing identical vectors consistently jointly harmonized together alongside globally shared underlying network weight parameters [21]. By strategically consistently amortizing embedded parameter mathematical representations globally via g_{θ_p} , this systematic parameterized manifold fusion paradigm reliably successfully evades profoundly exhaustive per-instance iterative test-time latent optimizations historically mandated explicitly adjusting for coefficient variability. Concurrently, it beneficially

exploits shared solution similarities broadly overlapping straightforward standard mathematical “easy” and stringently physically rigid essentially demanding mathematically stiff phenomenologically “hard” governing regimes fundamentally improving foundational training model general predictive stability systematically [41].

However, these parameterized manifolds prominently remain *static* in time, inherently treating time t merely as an identical spatial input coordinate, comprehensively confining the overall trained model rigidly over an exclusively fixed finite operational horizon [26]. Consequently, this standardized coordinate-regression formulation profoundly misses explicitly encoding an intrinsic dynamic mathematical system, drastically curtailing *Out-t* extrapolation capabilities securely extending meaningfully beyond the bounded mathematical training window [60, 52]. Furthermore, extrapolating toward demanding parameter regimes strictly falling completely outside the initial standardized training statistical distribution persists systematically challenging concerning structurally static generalized conditioning, predominantly occurring significantly whenever defining PDE system dynamics qualitatively completely fundamentally alter precisely across transitioning coefficient mathematical numerical ranges [26, 27]. Unambiguously, recognizing these cumulative architectural boundary limitations powerfully logically implicitly formally suggests that sequentially introducing robust explicitly isolated continuous continuous-time latent generative operational dynamics structural mechanisms undoubtedly remains imperatively critical systematically appropriately comprehensively securely enabling robustly completely functionally parameterized overarching global manifold predictive network mathematical structural continuous systemic unified fusion concurrently consistently accurately paired dynamically extensively alongside functional unified rigorous fundamentally reliable robust profound temporally deeply projected long-horizon mathematical forecasting explicitly.

3.4. Motivation

Parameterized manifold fusion can replace auto-decoding. Auto-decoding treats each instance as a separate optimization problem, where a latent code is iteratively updated, and meta-learning can be used to organize instance adaptation [36, 21, 32]. This instance-wise latent inference can be viewed as a multi-task learning procedure in which each task has its own latent variables [25, 44]. In contrast, parameterized manifold fusion encodes collocation coordinates and PDE parameters via separate encoders and fuses

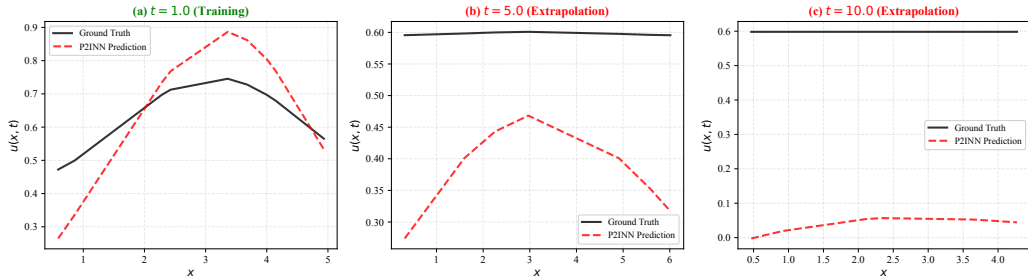


Figure 2: Comparison of ground truth (solid black) and P²INN prediction (dashed red) for $u(x, t)$ versus x at $t = 1.0$, $t = 5.0$, and $t = 10.0$.

them in a shared decoder, producing parameter-conditioned representations directly without per-instance iterative optimization [56, 26].

P²INN fails to extrapolate beyond the training horizon. Although P²INN [10] constructs a parameterized solution manifold and generalizes well to unseen PDE coefficients within the training time window, it treats time t as a static coordinate input rather than modeling intrinsic temporal dynamics. As a result, when queried at times $t > T_{\text{tr}}$, the model must extrapolate in time without an explicit dynamical structure, and its predictions degrade rapidly. Figure 2 illustrates this limitation: at $t = 1.0$ (within the training horizon), P²INN’s prediction follows the ground truth reasonably well; at $t = 5.0$ and $t = 10.0$ (extrapolation), the predicted solution deviates severely—failing to capture the flat, constant behavior and correct magnitude of the true solution, demonstrating extrapolation failure of P²INN. This empirical evidence underscores that static manifold fusion alone is insufficient for reliable *Out-t* extrapolation and motivates the need for explicit latent dynamics modeling conditioned on PDE parameters.

A more comprehensive view is given by multiple error metrics evaluated over the time horizon (Fig 4). The L_2 absolute error, L_2 relative error, and maximum error of P²INN all exhibit approximately linear growth as T increases beyond the training limit, while the explained variance score decreases approximately linearly (becoming more negative). Together, these four indicators consistently reveal that P²INN’s predictive quality degrades in a roughly linear fashion with extrapolation time, all metrics indicating extrapolation failure, reinforcing the limitation of static manifold fusion for long-horizon forecasting.

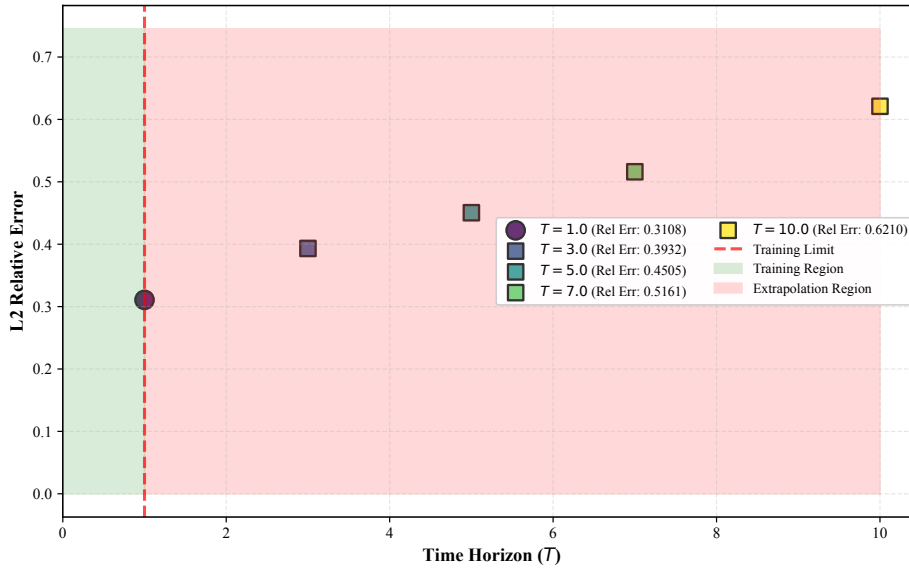


Figure 3: Growth of P²INN’s L_2 relative error over the time horizon T .

Latent space dynamic of parameterized PDEs may exist. Solutions under nearby PDE parameters often share common structures, suggesting that their evolution trajectories may lie on a low-dimensional manifold [26, 21]. Latent dynamics models show that continuous-time evolution can be captured efficiently by learning a latent ODE and decoding latent states to spatial fields [9, 8, 60]. This motivates modeling parameterized PDE evolution as a parameter-conditioned latent dynamics system that can be integrated continuously in time and reconstructed by a shared INR-style decoder [52, 60].

As shown in Fig 3, the L_2 relative error of P²INN exhibits an approximately linear increase with T in the extrapolation region, reflecting the absence of an intrinsic dynamical structure that would constrain error propagation over time, revealing the extrapolation failure of static coordinate-based regression. This growth characteristic further underscores the need for explicit latent dynamics modeling to achieve stable long-horizon prediction.

Disentangled space–time–parameter encodings may benefit dynamic manifold modulation. Space–time separation strategies in INRs, such as multiplicative modulation mechanisms, have been used to simplify sequence modeling and improve efficiency [14]. Fourier-feature-based parameteriza-

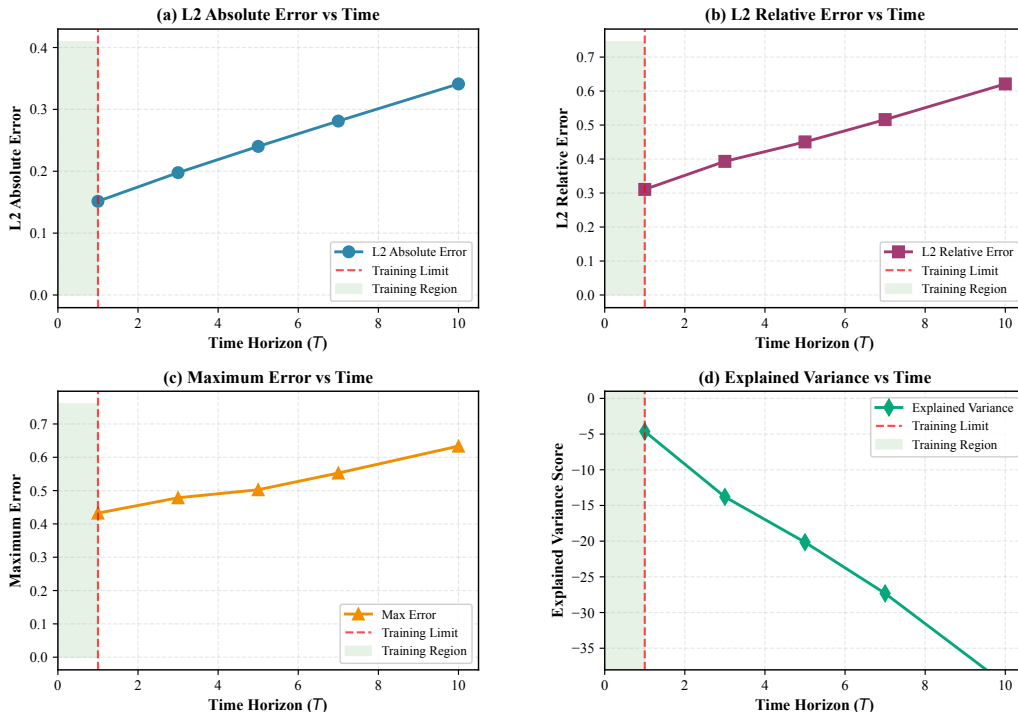


Figure 4: P²INN’s error metrics versus time horizon T . (a) L_2 absolute error, (b) L_2 relative error, (c) maximum error grow approximately linearly beyond the training limit; (d) explained variance decreases approximately linearly.

tions can be interpreted as modulating amplitudes and phases of wave components, which can be beneficial for representing oscillatory signals [14, 41]. However, directly factorizing time and space inside a single coordinate encoder may overlook the coupled nature of PDE dynamics and can lead to optimization difficulties in stiff regimes [26, 55]. This motivates constructing separate latent manifolds for space, time (as latent dynamics), and parameters, and performing fusion at the manifold network level to enable expressive interactions while maintaining stable training [60, 52, 26].

A more comprehensive view of P²INN’s error metrics over time is given in Fig 4. The L_2 absolute error, L_2 relative error, and maximum error of P²INN all exhibit approximately linear growth as T increases beyond the training limit, while the explained variance score decreases approximately linearly (becoming more negative). Together, these four indicators consistently reveal that P²INN’s predictive quality degrades in a roughly linear fashion with

extrapolation time, all metrics indicating extrapolation failure, reinforcing the limitation of static manifold fusion for long-horizon forecasting.

4. Method

We propose Disentangled Latent Dynamics Manifold Fusion (DLDMF), a physics-informed solver for families of time-dependent parameterized PDEs. The core idea is to disentangle *space*, *time*, and *PDE parameters* into three separate manifolds, and to fuse them only at a shared continuous decoder, while modeling time evolution intrinsically via a parameter-conditioned latent Neural ODE. Unlike latent-space dynamics pipelines that require per-instance auto-decoding to infer latent states (i.e., test-time iterative optimization), DLDMF initializes its latent dynamics through a feed-forward mapping from PDE parameters, avoiding iterative inference at deployment.

4.1. Model Architecture

DLDMF aims to approximate the solution operator of a parameterized PDE family, $u(x, t; \boldsymbol{\mu})$, by combining (i) a parameter manifold encoder, (ii) a spatial manifold encoder, (iii) a latent dynamics manifold evolving in continuous time, and (iv) a manifold fusion decoder.

Disentangled parameter and spatial manifolds. We encode PDE parameters $\boldsymbol{\mu}$ and spatial coordinates x using two separate encoders:

$$\mathbf{h}_{\text{param}} = g_{\theta_p}(\boldsymbol{\mu}), \quad (7)$$

$$\mathbf{h}_x = g_{\theta_x}(x). \quad (8)$$

where $\mathbf{h}_{\text{param}} \in \mathbb{R}^{d_p}$ represents the *parameterized solution manifold coordinate* and $\mathbf{h}_x \in \mathbb{R}^{d_x}$ represents the *spatial manifold coordinate*. This preserves the key benefit of parameterized manifold conditioning in P²INN-style designs, i.e., representing a family of PDEs without retraining from scratch for each new $\boldsymbol{\mu}$.

Latent dynamics manifold fusion. Instead of treating time t as a coordinate input to the decoder, DLDMF represents time via a latent state $\mathbf{z}_t \in \mathbb{R}^{d_z}$ that evolves according to a parameter-conditioned Neural ODE [9].

We generate the initial latent state by a feed-forward mapping conditioned on PDE parameters without auto-decoding:

$$\mathbf{z}_0 = g_{\theta_0}(\mathbf{h}_{\text{param}}), \quad (9)$$

which removes the need for solving an inverse problem by iterative auto-decoding at inference time.

We define the continuous-time latent dynamics evolution as

$$\frac{d\mathbf{z}_t}{dt} = f_{\theta_f}(\mathbf{z}_t, \mathbf{h}_{\text{param}}), \quad \mathbf{z}_t = \text{ODESolve}(f_{\theta_f}, \mathbf{z}_0, t; \mathbf{h}_{\text{param}}), \quad (10)$$

where $\text{ODESolve}(\cdot)$ is a differentiable numerical integrator. This continuous-time formulation naturally supports querying at arbitrary t and enables *Out-t* extrapolation by integrating beyond the training horizon [60, 52].

Finally, DLDMF reconstructs the PDE solution by fusing the three disentangled manifolds in the decoder:

$$\hat{u}(x, t; \boldsymbol{\mu}) = g_{\theta_g}([\mathbf{h}_x; \mathbf{z}_t; \mathbf{h}_{\text{param}}]), \quad (11)$$

where g_{θ_g} is a coordinate-based manifold network (INR decoder) that is continuous in x and can be evaluated on arbitrary grids. We denote the full parameter set as

$$\Theta = \{\theta_x, \theta_p, \theta_0, \theta_f, \theta_g\}. \quad (12)$$

Time derivatives through latent dynamics. Since t influences \hat{u} only through \mathbf{z}_t , the time derivative required by PDE residuals is computed via the chain rule:

$$\partial_t \hat{u}(x, t; \boldsymbol{\mu}) = \frac{\partial g_{\theta_g}}{\partial \mathbf{z}}([\mathbf{h}_x; \mathbf{z}_t; \mathbf{h}_{\text{param}}]) \cdot \frac{d\mathbf{z}_t}{dt} = \frac{\partial g_{\theta_g}}{\partial \mathbf{z}}(\cdot) \cdot f_{\theta_f}(\mathbf{z}_t, \mathbf{h}_{\text{param}}). \quad (13)$$

while spatial derivatives (e.g., $\nabla_x \hat{u}$, $\nabla_x^2 \hat{u}$) are obtained by automatic differentiation through $\mathbf{h}_x = g_{\theta_x}(x)$ and the decoder.

4.2. Pre-training

DLDMF is trained with standard physics-informed objectives by minimizing PDE residuals and enforcing initial/boundary conditions. Let $\mathcal{C}_f^{(i)}$, $\mathcal{C}_u^{(i)}$, and $\mathcal{C}_b^{(i)}$ denote collocation sets for PDE residual, initial condition, and boundary condition for parameter instance $\boldsymbol{\mu}_i$, respectively. We define the physics residual

$$r_{\Theta}(x, t; \boldsymbol{\mu}) = \mathcal{F}(x, t, \hat{u}, \partial_t \hat{u}, \nabla_x \hat{u}, \nabla_x^2 \hat{u}; \boldsymbol{\mu}), \quad (14)$$

where $\partial_t \hat{u}$ is computed by Eq. (13). The overall training objective is

$$L(\Theta) = w_1 L_u + w_2 L_f + w_3 L_b, \quad (15)$$

with

$$L_f = \frac{1}{|\mathcal{B}|} \sum_{i \in \mathcal{B}} \frac{1}{|\mathcal{C}_f^{(i)}|} \sum_{(x,t) \in \mathcal{C}_f^{(i)}} \|r_{\Theta}(x, t; \boldsymbol{\mu}_i)\|_2^2, \quad (16)$$

$$L_u = \frac{1}{|\mathcal{B}|} \sum_{i \in \mathcal{B}} \frac{1}{|\mathcal{C}_u^{(i)}|} \sum_{x \in \mathcal{C}_u^{(i)}} \|\hat{u}(x, 0; \boldsymbol{\mu}_i) - u_0(x; \boldsymbol{\mu}_i)\|_2^2, \quad (17)$$

$$L_b = \frac{1}{|\mathcal{B}|} \sum_{i \in \mathcal{B}} \frac{1}{|\mathcal{C}_b^{(i)}|} \sum_{(x,t) \in \mathcal{C}_b^{(i)}} \|\mathcal{B}(x, t, \hat{u}, \nabla_x \hat{u}; \boldsymbol{\mu}_i)\|_2^2. \quad (18)$$

where \mathcal{B} denotes a mini-batch of parameter instances and $w_1, w_2, w_3 \in \mathbb{R}$ are hyperparameters. Compared to vanilla PINNs trained for a single PDE instance, we minimize losses over multiple $\boldsymbol{\mu}_i$ in each iteration, which directly targets parameterized learning and avoids retraining from scratch for each new coefficient configuration.

4.3. Fast Fine-tuning

As the ultimate goal of this study is to deploy trained models to a set of specific PDE parameters of interest, we devise a method to fine-tune the trained models to improve solution accuracy at those query PDE parameters. To this end, we adopt an idea of SVD-PINNs [17], which shows that extracting basis through singular value decomposition (SVD) from the weights of a PINN trained on a single PDE equation is effective in transferring information. Extending this insight, we introduce an *SVD modulation* by obtaining bases through applying SVD to the weights of the decoder layers of DLDMF. Specifically, only the manifold network g_{θ_g} is transformed to a form that can be modulated. Each layer, excluding the first and last layers, is decomposed as follows

$$FC_l = \Psi_l \alpha_l \Phi_l^T, \quad l = 2, 3, \dots, D_g - 1. \quad (19)$$

Then, during fine-tuning, we set $\{\alpha_l\}_{l=2}^{D_g-1}$ to be learnable, while keeping all other parameters in the network fixed. It is an option to fix the parameters of FC_1 and FC_{D_g} .

For INR, the *shift modulation* [13] has been one of the leading architectural choices. However, we found empirically that modulating by shift in PINNs does not lead to significant performance improvement.

4.4. Extrapolation

For a new PDE parameter set $\boldsymbol{\mu}^*$, potentially outside the training range, DLDMF computes by

$$\mathbf{h}_{\text{param}}^* = g_{\theta_p}(\boldsymbol{\mu}^*), \quad (20)$$

$$\mathbf{z}_0^* = \Phi_{\theta_0}(\mathbf{h}_{\text{param}}^*), \quad (21)$$

$$\mathbf{z}_t^* = \text{ODESolve}(F_{\theta_f}, \mathbf{z}_0^*, t; \mathbf{h}_{\text{param}}^*). \quad (22)$$

where evolves \mathbf{z}_t^* via Eq. (10) for any $t \in [0, T']$ (including $t > T_{\text{tr}}$), and decodes $\hat{u}(x, t; \boldsymbol{\mu}^*)$ via Eq. (11). This procedure involves only feed-forward computation and ODE integration, supporting both parameter extrapolation and time extrapolation without iterative latent inference.

5. Experiments

We evaluate the proposed DLDMF method on a series of parametric time-dependent PDE benchmarks. Our experiments aim to assess whether disentangling parameter, spatial representation, and latent temporal dynamics—and subsequently fusing them through a unified manifold decoder—leads to improved generalization, stability, and adaptability compared to existing neural PDE solvers.

5.1. Benchmarks

Parameterized CDR equations (1D). Our primary benchmark is the parameterized Convection–Diffusion–Reaction (CDR) family

$$\frac{\partial u}{\partial t} + \beta \frac{\partial u}{\partial x} - \nu \frac{\partial^2 u}{\partial x^2} - \rho u(1 - u) = 0, \quad x \in \Omega, \quad t \in [0, T]. \quad (23)$$

which exhibits qualitatively different behaviors across coefficients (β, ν, ρ) and contains regimes that are notoriously hard for standard PINN optimization [26]. We use the CDR family to probe whether a single learned solver can (i) generalize across coefficient configurations, (ii) extrapolate beyond the training time window, and (iii) remain stable in hard regimes where strong convection or reaction creates sharp transitions or high-frequency oscillations [26]. Reference solutions for evaluation are generated by standard numerical solvers; for 1D splitting-based construction, we follow classical operator-splitting practice [50].

Higher-dimensional spatiotemporal PDEs (2D). To test whether the proposed manifold fusion with latent dynamics scales beyond 1D toy problems, we additionally consider a 2D fluid benchmark based on incompressible Navier–Stokes dynamics under the commonly used forced turbulence setting from prior learning-based PDE studies. We treat the Reynolds number (or viscosity-related coefficient) as the PDE parameter, so that the evaluation explicitly measures parameter generalization and parameter extrapolation in a regime where long-horizon forecasting is challenging.

Datasets splits and time extrapolation. For each benchmark, we split the temporal domain into a training horizon $[0, T_{\text{tr}}]$ and an extended inference horizon $[0, T_{\text{ts}}]$ with $T_{\text{ts}} > T_{\text{tr}}$ to evaluate *In-t* and *Out-t* performance [60, 52]. To evaluate parameter generalization, we sample parameter configurations in a training set \mathcal{P}_{tr} and test on (i) *interpolation* parameters inside the convex hull of \mathcal{P}_{tr} and (ii) *extrapolation* parameters outside this range. We also consider *joint* stress tests where both $t > T_{\text{tr}}$ and $\boldsymbol{\mu} \notin \mathcal{P}_{\text{tr}}$.

5.2. Baselines

The empirical evaluation includes representative methods that address parametric PDE modeling from distinct architectural perspectives.

Parameter-conditioned physics-informed architectures are represented by P²INN [10] and PI-DeepONet [56]. P²INN introduces an explicit encoder for PDE coefficients and integrates parameter representations into a shared solution network. PI-DeepONet extends operator learning with physics-informed regularization and learns mappings conditioned on both initial states and coefficients. These approaches provide reference points for parameter-aware operator approximation under physics constraints.

Continuous-time latent dynamics models are included through DINO [60] and PIDO [52], both of which evolve latent representations via Neural ODE formulations [9]. These models emphasize temporal consistency through continuous integration and have demonstrated strong performance in long-horizon forecasting. In most formulations, parameter information and spatial encoding are embedded within a unified latent state, and instance-specific inference may involve auto-decoding mechanisms [36].

Meta-learning-based solvers are represented by MAD [21], which leverages cross-task pre-training to accelerate adaptation to new parameter instances. Its formulation focuses on rapid fine-tuning across task distributions rather

than constructing a globally shared parameter-conditioned dynamics manifold.

All baseline models are trained under comparable settings using publicly available implementations or carefully reimplemented versions consistent with their original specifications.

5.3. Evaluation and metrics

Accuracy metrics. We evaluate solution quality using the L_2 relative error $\|\hat{\mathbf{u}} - \mathbf{u}\|_2 / \|\mathbf{u}\|_2$ and, when informative, the absolute L_2 error. Errors are computed on a dense evaluation grid over (x, t) for each test parameter configuration and then aggregated across the test set. To separate short-horizon fitting from long-horizon extrapolation, we report errors on *In-t* ($t \leq T_{\text{tr}}$) and *Out-t* ($t > T_{\text{tr}}$) intervals.

Temporal extrapolation (*Out-t*). DLDMF produces $\hat{u}(x, t; \boldsymbol{\mu})$ at arbitrary t by integrating its parameter-conditioned latent ODE and decoding via manifold fusion, so *Out-t* evaluation is performed by directly querying $t \in (T_{\text{tr}}, T_{\text{ts}}]$. For baselines that do not natively output beyond the training horizon, we adopt a standard iterative extension protocol: the last predicted state within the training horizon is treated as the initial condition for the next window, and the model is rolled forward repeatedly to reach T_{ts} .

Parameterized extrapolation (*Out- $\boldsymbol{\mu}$*). We assess generalization to unseen parameters via two regimes: interpolation inside the training range and extrapolation outside the training range, following prior parameterized PDE evaluations. This evaluation is conducted for both *In-t* and *Out-t* horizons to test whether temporal extrapolation remains stable when coefficients shift.

5.4. Implementation details

Training signal and supervision. DLDMF is trained with physics-informed objectives using PDE residuals and initial/boundary constraints, following the PINN training formalism. For parameterized training, we mini-batch over PDE parameter instances and their associated collocation points, so that each optimization step mixes multiple $\boldsymbol{\mu}$ values and encourages a shared parameterized representation.

Neural ODE solver. We use a differentiable ODE solver to integrate the latent dynamics in continuous time, enabling evaluation at arbitrary temporal resolutions and beyond the training horizon. To ensure a fair comparison, we maintain consistency in solver type and tolerances across ODE-based baselines.

Reproducibility. All reported metrics are averaged over multiple random seeds, and we keep network capacity and training budgets comparable across methods whenever possible to focus the evaluation on modeling assumptions rather than scale.

5.5. Main results

To assess the models’ capability to predict past the training horizon, we adopt the auto-regressive evaluation strategy from [53] for PI-DeepONet and MAD. This approach iteratively extends forecasts by using the final state predicted in the training interval as the initial condition for the next one. As shown in Table 1, across all scenarios, DLDMF demonstrates clear superiority over the baseline methods on both *In-t* and *Out-t*. In particular, DLDMF achieves the lowest L_2 relative errors on the test set, with 1.89% for *In-t* and 4.21% for *Out-t*, significantly outperforming all baselines. While P²INN suffers from the lack of intrinsic temporal dynamics (21.34% and 32.87% on test *In-t* and *Out-t*, respectively), as illustrated by its extrapolation failure in Fig. 2, PIDO and DINO show competitive performance but still cannot match the robustness of DLDMF in long-term extrapolation.

5.6. Ablation studies

We design ablations to isolate the contribution of each component of DLDMF.

Impact of latent dynamics. We replace the latent ODE time representation with a direct time encoder (i.e., treat t as an input coordinate) while keeping the parameter and spatial encoders identical, yielding a static manifold-fusion baseline analogous to parameterized PINNs. This ablation measures whether explicit dynamics modeling is necessary for *Out-t* extrapolation.

Impact of manifold fusion. We compare the full disentangled fusion (space, time, and parameters fused at the latent space) against variants that entangle subsets of variables, to test whether separation improves stability and extrapolation.

Table 1: Comparison with DLDMF trained with different sub-sampling ratios of training set. L_2 relative error is reported (%).

MODEL	DATASET	TRAIN		TEST	
		IN-T	OUT-T	IN-T	OUT-T
DLDMF	-	1.35	3.15	1.89	4.21
P ² INN	-	8.45	15.23	21.34	32.87
PIDO	-	1.58	3.89	5.67	8.94
DINO	100%	1.42	3.32	4.89	6.52
DINO	50%	1.14	4.90	5.25	8.76
DINO	25%	0.82	7.52	7.37	13.58
DINO	12.5%	0.47	13.59	15.12	31.74

To quantify the practical impact of eliminating auto-decoding, we implement a variant that infers the initial forward latent state using the standard auto-decoding optimization procedure. We evaluate both accuracy and computational overhead under the same decoding loss and stopping criteria to highlight the trade-off between iterative inference and amortized initialization.

5.7. Computational efficiency

Because a key motivation of DLDMF is to support multi-query evaluation without test-time iterative optimization, we report efficiency metrics alongside accuracy. Specifically, we measure (i) inference latency per parameter query, (ii) the number of gradient steps required at inference for methods that use auto-decoding, and (iii) memory overhead associated with storing per-instance latent codes in instance-parameterized methods. This analysis complements accuracy metrics by quantifying the deployment cost of parameterized PDE solvers in real-time and high-throughput settings.

6. Discussion

Auto-decoding as an inverse problem: structural limitations. Auto-decoding reformulates latent inference as an inverse optimization problem.

Given a trained decoder g_{θ_g} , the latent variable for a new instance is obtained by solving

$$\mathbf{z}^* = \arg \min_{\mathbf{z}} \|g_{\theta_g}(\mathbf{z}) - u\|^2. \quad (24)$$

This formulation has two fundamental implications.

First, inference is no longer a feed-forward mapping but a non-convex optimization process. The recovered latent state depends on initialization and local curvature of the loss landscape. For nonlinear PDEs, especially those exhibiting stiffness or chaotic sensitivity, small deviations in the inferred \mathbf{z}^* lead to exponentially amplified errors during latent ODE rollout.

Second, auto-decoding does not learn a global parameter-to-manifold mapping. Each latent vector is optimized independently, which yields a set of discrete codes rather than a continuous embedding of the parameter space. As a result, the latent geometry lacks guaranteed smoothness across parameter variations. This discontinuity becomes critical when latent trajectories are evolved by Neural ODEs: the learned vector field may drive trajectories into poorly supported regions of latent space, producing unstable long-time extrapolation.

Thus, the limitation of auto-decoding is not merely computational inefficiency. It is geometric: the latent manifold is not explicitly constructed as a parameterized continuous object.

Time extrapolation under latent initialization bias. In latent Neural ODE frameworks such as DINO [60] and PIDO [52], time evolution is modeled as

$$\frac{d\mathbf{z}_t}{dt} = f_{\theta_f}(\mathbf{z}_t), \quad (25)$$

However, the initial state \mathbf{z}_0 is obtained via auto-decoding. Hence, the entire trajectory is conditioned on a solution to a non-convex inverse problem.

For dissipative or convection-dominated PDEs, the solution operator may exhibit strong sensitivity to initial conditions. If \mathbf{z}_0 deviates from the true manifold coordinate, the error propagates according to the stability properties of the learned vector field. When the system is marginally stable or stiff, this leads to rapid degradation in Out-of-Time extrapolation.

In contrast, DLDMF defines

$$\mathbf{z}_0 = g_{\theta_0}(\mathbf{h}_{\text{param}}), \quad \frac{d\mathbf{z}_t}{dt} = f_{\theta_f}(\mathbf{z}_t, \mathbf{h}_{\text{param}}). \quad (26)$$

where $\mathbf{h}_{\text{param}}$ is a continuous encoding of PDE parameters. The initial state is no longer inferred from data but generated from a deterministic mapping on the parameter manifold. Consequently, the latent trajectory remains consistent with the global geometry of the parameterized solution manifold. Time extrapolation becomes a property of the learned flow, not of inverse optimization.

Meta-auto-decoding and bi-level instability. MAD introduces a meta-auto-decoding framework in which a solution manifold is pre-learned and adaptation to new PDE instances is achieved by optimizing latent variables, optionally together with model parameters (MAD-LM).

This procedure implicitly defines a bi-level optimization:

$$\min_{\Theta} \sum_i \min_{\mathbf{z}_i} \mathcal{L}(u_{\Theta}(\cdot, \mathbf{z}_i); \boldsymbol{\mu}_i), \quad (27)$$

While avoiding explicit second-order differentiation, this nested structure introduces adaptation instability.

When PDE parameters strongly affect stiffness or spectral complexity, latent-only adaptation (MAD-L) may fail to represent new regimes. Joint adaptation (MAD-LM) partially resolves this by updating Θ , but at the cost of additional optimization loops and loss of strict parameter consistency. The adapted model effectively deforms the learned manifold locally, which undermines global coherence across parameter space.

DLDMF removes the bi-level structure entirely. Parameter generalization is achieved through explicit encoding, and latent dynamics are shared across all instances. The optimization objective becomes single-stage:

$$\min_{\Theta} \mathcal{L}(\hat{u}_{\Theta}(x, t; \boldsymbol{\mu})). \quad (28)$$

This structural simplification enhances stability and preserves manifold continuity across parameter ranges.

From static to dynamic manifold fusion. P²INN introduced static manifold fusion, where parameter embeddings and spatial coordinates are fused in a shared decoder. Time, however, remains an explicit coordinate input, which leads to severe extrapolation failure beyond the training horizon (see Fig. 2).

This design implicitly assumes that the solution manifold can be represented as

$$u(x, t; \boldsymbol{\mu}) = g_{\theta_g}(x, t; \boldsymbol{\mu}), \quad (29)$$

where t is treated symmetrically with spatial coordinates. Such a formulation models temporal behavior as interpolation within the training horizon.

DLDMF replaces coordinate-based temporal modeling with intrinsic manifold evolution:

$$\hat{u}(x, t; \boldsymbol{\mu}) = g_{\theta_g}(\mathbf{h}_x, \mathbf{z}_t, \mathbf{h}_{\text{param}}). \quad (30)$$

Here, time is no longer an input coordinate but a trajectory on a parameter-conditioned latent manifold. This transforms static fusion into dynamic fusion.

Conceptually, this shift aligns the representation with the mathematical structure of PDEs, which define flows in function space. The learned vector field approximates the generator of this flow. Therefore, temporal extrapolation becomes an integration problem rather than a coordinate regression problem.

Parameter-induced stiffness and spectral bias. A central difficulty in parameterized PDE learning is that parameters often alter not only solution magnitude but also spectral content. For instance, decreasing viscosity or increasing convection coefficients introduces high-frequency modes. This intensifies spectral bias in MLP-based solvers, which preferentially learn low-frequency components.

Auto-decoding partially mitigates this by overfitting latent codes per instance, but it does not resolve spectral bias structurally. Moreover, under parameter shifts, the latent space may not capture new spectral regimes.

Dynamic manifold fusion offers a distinct mechanism. Because the vector field is conditioned continuously on parameter embeddings, the learned dynamics can adjust how high-frequency components evolve. This decouples parameter-induced stiffness from coordinate-based regression difficulty.

To our knowledge, DLDMF is the first physics-informed framework that unifies: (i) explicit parameter manifold encoding, (ii) intrinsic continuous-time latent dynamics, and (iii) elimination of test-time optimization, thereby addressing parameter-induced stiffness and long-term temporal extrapolation within a single coherent geometric model.

7. Conclusion

In this paper, we propose Disentangled Latent Dynamics Manifold Fusion (DLDMF), a novel physics-informed framework for efficiently solving parameterized partial differential equations (PDEs). While existing physics-informed neural networks offer a promising mesh-free paradigm, they typically require time-consuming repetitive training and struggle with parameter-induced stiffness. Furthermore, extending these models to perform reliable long-term temporal extrapolation remains a formidable challenge. Although recent latent dynamics approaches address continuous time evolution, they rely heavily on instance-wise iterative auto-decoding. This inverse optimization incurs prohibitive test-time computational costs and fundamentally disrupts the continuous geometry of the parameterized solution space.

To overcome these critical limitations, DLDMF introduces a principled space-time-parameter disentanglement strategy. By replacing unstable auto-decoding with a deterministic feed-forward mapping, our model explicitly encodes PDE coefficients to initialize a continuous temporal latent state. This evolution is intrinsically governed by a parameter-conditioned Neural ODE. Subsequently, a dynamic manifold fusion mechanism seamlessly integrates the disentangled spatial coordinates, parameter embeddings, and time-evolving latent states, explicitly decoding them into physically consistent solutions. By shifting from static coordinate regression to intrinsic dynamic flow integration, DLDMF structurally decouples parameter-induced spectral bias from temporal dynamics.

Extensive experiments on challenging benchmarks, including 1D convection-diffusion-reaction and 2D Navier-Stokes equations, demonstrate that DLDMF significantly outperforms state-of-the-art baselines. Our approach achieves robust parameter generalization and exceptional long-term temporal extrapolation without requiring any test-time latent optimization. Moreover, the proposed SVD-based fast fine-tuning strategy enables highly efficient adaptation to query parameters.

For future work, extending DLDMF to handle diverse boundary conditions and irregular spatial geometries represents a crucial next step. Scaling this framework to large-scale, real-world physical systems is an exciting avenue.

References

- [1] Martín Abadi, Paul Barham, Jianmin Chen, Zhifeng Chen, Andy Davis, Jeffrey Dean, Matthieu Devin, Sanjay Ghemawat, Geoffrey Irving, Michael Isard, et al. {TensorFlow}: A system for {Large-Scale} machine learning. In *12th USENIX symposium on operating systems design and implementation (OSDI 16)*, pages 265–283, 2016.
- [2] Ibrahim Ayed, Emmanuel de Bézenac, Arthur Pajot, Julien Brajard, and Patrick Gallinari. Learning dynamical systems from partial observations. *arXiv preprint arXiv:1902.11136*, 2019.
- [3] Nathan Baker, Frank Alexander, Timo Bremer, Aric Hagberg, Yannis Kevrekidis, Habib Najm, Manish Parashar, Abani Patra, James Sethian, Stefan Wild, et al. Workshop report on basic research needs for scientific machine learning: Core technologies for artificial intelligence. Technical report, USDOE Office of Science (SC), Washington, DC (United States), 2019.
- [4] Peter W Battaglia, Jessica B Hamrick, Victor Bapst, Alvaro Sanchez-Gonzalez, Vinicius Zambaldi, Mateusz Malinowski, Andrea Tacchetti, David Raposo, Adam Santoro, Ryan Faulkner, et al. Relational inductive biases, deep learning, and graph networks. *arXiv preprint arXiv:1806.01261*, 2018.
- [5] Atilim Gunes Baydin, Barak A Pearlmutter, Alexey Andreyevich Radul, and Jeffrey Mark Siskind. Automatic differentiation in machine learning: a survey. *Journal of Machine Learning Research*, 18:1–43, 2018.
- [6] Johannes Brandstetter, Daniel E Worrall, and Max Welling. Message passing neural pde solvers. In *International Conference on Learning Representations*, 2021.
- [7] Hao Chen, Bo He, Hanyu Wang, Yixuan Ren, Ser Nam Lim, and Abhinav Shrivastava. NeRV: Neural representations for videos. In Marc’Aurelio Ranzato, Alina Beygelzimer, Yann Dauphin, Percy Liang, and Jenn Wortman Vaughan, editors, *Advances in Neural Information Processing Systems*, volume 34, pages 21557–21568. Curran Associates, Inc., 2021.

- [8] Peter Yichen Chen, Jinxu Xiang, Dong Heon Cho, Yue Chang, G A Pershing, Henrique Teles Maia, Maurizio M. Chiaramonte, Kevin Thomas Carlberg, and Eitan Grinspun. CROM: Continuous reduced-order modeling of PDEs using implicit neural representations. In *International Conference on Learning Representations*, 2023.
- [9] Ricky TQ Chen, Yulia Rubanova, Jesse Bettencourt, and David K Duvenaud. Neural ordinary differential equations. *Advances in Neural Information Processing Systems*, 31, 2018.
- [10] Woojin Cho, Minju Jo, Haksoo Lim, Kookjin Lee, Dongeun Lee, Sanghyun Hong, and Noseong Park. Parameterized physics-informed neural networks for parameterized pdes. *arXiv preprint arXiv:2408.09446*, 2024.
- [11] Miles Cranmer, Sam Greydanus, Stephan Hoyer, Peter Battaglia, David Spergel, and Shirley Ho. Lagrangian neural networks. In *ICLR 2020 Workshop*, 2020.
- [12] Miles Cranmer, Sam Greydanus, Stephan Hoyer, Peter Battaglia, David Spergel, and Shirley Ho. Lagrangian neural networks, 2020.
- [13] Emilien Dupont, Hyunjik Kim, S. M. Ali Eslami, Danilo Jimenez Rezende, and Dan Rosenbaum. From data to functa: Your data point is a function and you can treat it like one. In *39th International Conference on Machine Learning (ICML)*, 2022.
- [14] Rizal Fathony, Anit Kumar Sahu, Devin Willmott, and J Zico Kolter. Multiplicative filter networks. In *International Conference on Learning Representations*, 2020.
- [15] Stefania Fresca, Andrea Manzoni, Luca Dedè, and Alfio Quarteroni. Deep learning-based reduced order models in cardiac electrophysiology. *PLoS ONE*, 15(10), October 2020.
- [16] Stefania Fresca, Andrea Manzoni, Luca Dedè, and Alfio Quarteroni. Deep learning-based reduced order models in cardiac electrophysiology. *PLoS ONE*, 15(10), October 2020.

- [17] Yihang Gao, Ka Chun Cheung, and Michael K. Ng. Svd-pinns: Transfer learning of physics-informed neural networks via singular value decomposition. In *2022 IEEE Symposium Series on Computational Intelligence (SSCI)*. IEEE, December 2022.
- [18] Víctor Garcia Satorras, Emiel Hoogeboom, and Max Welling. E(n) equivariant graph neural networks. In *Proceedings of the 38th International Conference on Machine Learning*, volume 139 of *Proceedings of Machine Learning Research*, pages 9323–9332. PMLR, 2021.
- [19] Daniel Greenfeld, Meirav Galun, Ronen Basri, Irad Yavneh, and Ron Kimmel. Learning to optimize multigrid pde solvers. In *International Conference on Machine Learning*, pages 2415–2423. PMLR, 2019.
- [20] Samuel Greydanus, Misko Dzamba, and Jason Yosinski. Hamiltonian neural networks. *Advances in Neural Information Processing Systems*, 32:15379–15389, 2019.
- [21] Xiang Huang, Zhanhong Ye, Hongsheng Liu, Shi Ji, Zidong Wang, Kang Yang, Yang Li, Min Wang, Haotian Chu, Fan Yu, et al. Meta-auto-decoder for solving parametric partial differential equations. *Advances in Neural Information Processing Systems*, 35:23426–23438, 2022.
- [22] Ameya D Jagtap and George Em Karniadakis. Extended physics-informed neural networks (xpinns): A generalized space-time domain decomposition based deep learning framework for nonlinear partial differential equations. *Communications in Computational Physics*, 28(5):2002–2041, 2020.
- [23] Ameya D Jagtap, Ehsan Kharazmi, and George Em Karniadakis. Conservative physics-informed neural networks on discrete domains for conservation laws: Applications to forward and inverse problems. *Computer Methods in Applied Mechanics and Engineering*, 365:113028, 2020.
- [24] George Em Karniadakis, Ioannis G Kevrekidis, Lu Lu, Paris Perdikaris, Sifan Wang, and Liu Yang. Physics-informed machine learning. *Nature Reviews Physics*, 3(6):422–440, 2021.
- [25] Alex Kendall, Yarin Gal, and Roberto Cipolla. Multi-task learning using uncertainty to weigh losses for scene geometry and semantics. In *Proceed-*

- ings of the IEEE conference on computer vision and pattern recognition*, pages 7482–7491, 2018.
- [26] Aditi Krishnapriyan, Amir Gholami, Shandian Zhe, Robert Kirby, and Michael W Mahoney. Characterizing possible failure modes in physics-informed neural networks. *Advances in Neural Information Processing Systems*, 34, 2021.
 - [27] Samuel Lanthaler, Roberto Molinaro, Patrik Hadorn, and Siddhartha Mishra. Nonlinear reconstruction for operator learning of pdes with discontinuities. In *The Eleventh International Conference on Learning Representations*, 2022.
 - [28] Kookjin Lee and Kevin T Carlberg. Deep conservation: A latent-dynamics model for exact satisfaction of physical conservation laws. In *Proceedings of the AAAI Conference on Artificial Intelligence*, volume 35, pages 277–285, 2021.
 - [29] Kookjin Lee, Nathaniel Trask, and Panos Stinis. Machine learning structure preserving brackets for forecasting irreversible processes. *Advances in Neural Information Processing Systems*, 34, 2021.
 - [30] Long Yuan Li and Peter Bettess. Adaptive finite element methods: A review. *Applied Mechanics Reviews*, 50(10):581–591, 1997.
 - [31] Zongyi Li, Nikola Borislavov Kovachki, Kamyar Azizzadenesheli, Kaushik Bhattacharya, Andrew Stuart, Anima Anandkumar, et al. Fourier neural operator for parametric partial differential equations. In *International Conference on Learning Representations*, 2020.
 - [32] Xu Liu, Xiaoya Zhang, Wei Peng, Weien Zhou, and Wen Yao. A novel meta-learning initialization method for physics-informed neural networks. *Neural Computing and Applications*, pages 1–24, 2022.
 - [33] Lu Lu, Pengzhan Jin, Guofei Pang, Zhongqiang Zhang, and George Em Karniadakis. Learning nonlinear operators via deeponet based on the universal approximation theorem of operators. *Nature machine intelligence*, 3(3):218–229, 2021.

- [34] Michael Lutter, Christian Ritter, and Jan Peters. Deep lagrangian networks: Using physics as model prior for deep learning. In *International Conference on Learning Representations*, 2018.
- [35] Peter J. Olver. *Introduction to partial differential equations*. Undergraduate Texts in Mathematics. Springer Cham, 2014.
- [36] Jeong Joon Park, Peter Florence, Julian Straub, Richard Newcombe, and Steven Lovegrove. DeepSDF: Learning continuous signed distance functions for shape representation. In *Proceedings of the IEEE/CVF conference on computer vision and pattern recognition*, pages 165–174, 2019.
- [37] Jeong Joon Park, Peter Florence, Julian Straub, Richard Newcombe, and Steven Lovegrove. DeepSDF: Learning continuous signed distance functions for shape representation. In *IEEE Conference on Computer Vision and Pattern Recognition (CVPR)*, pages 165–174, June 2019.
- [38] Adam Paszke, Sam Gross, Francisco Massa, Adam Lerer, James Bradbury, Gregory Chanan, Trevor Killeen, Zeming Lin, Natalia Gimelshein, Luca Antiga, et al. PyTorch: An imperative style, high-performance deep learning library. *Advances in neural information processing systems*, 32, 2019.
- [39] Kailash C Patidar. Nonstandard finite difference methods: recent trends and further developments. *Journal of Difference Equations and Applications*, 22(6):817–849, 2016.
- [40] Alessio Quaglino, Marco Gallieri, Jonathan Masci, and Jan Koutník. Snode: Spectral discretization of neural odes for system identification. In *International Conference on Learning Representations*, 2019.
- [41] Nasim Rahaman, Aristide Baratin, Devansh Arpit, Felix Draxler, Min Lin, Fred Hamprecht, Yoshua Bengio, and Aaron Courville. On the spectral bias of neural networks. In *International Conference on Machine Learning*, pages 5301–5310. PMLR, 2019.
- [42] Maziar Raissi, Paris Perdikaris, and George E Karniadakis. Physics-informed neural networks: A deep learning framework for solving forward and inverse problems involving nonlinear partial differential equations. *Journal of Computational Physics*, 378:686–707, 2019.

- [43] Keith Rudd and Silvia Ferrari. A constrained integration (cint) approach to solving partial differential equations using artificial neural networks. *Neurocomputing*, 155:277–285, 2015.
- [44] Sebastian Ruder. An overview of multi-task learning in deep neural networks. *arXiv preprint arXiv:1706.05098*, 2017.
- [45] Aleksei Sholokhov, Yuying Liu, Hassan Mansour, and Saleh Nabi. Physics-informed neural ode (pinode): embedding physics into models using collocation points. *Scientific Reports*, 13(1):10166, 2023.
- [46] Khemraj Shukla, Ameya D Jagtap, and George Em Karniadakis. Parallel physics-informed neural networks via domain decomposition. *Journal of Computational Physics*, 447:110683, 2021.
- [47] Vincent Sitzmann, Julien Martel, Alexander Bergman, David Lindell, and Gordon Wetzstein. Implicit neural representations with periodic activation functions. *Advances in Neural Information Processing Systems*, 33:7462–7473, 2020.
- [48] Ivan Skorokhodov, Sergey Tulyakov, and Mohamed Elhoseiny. StyleGAN-V: A continuous video generator with the price, image quality and perks of StyleGAN2. In *IEEE/CVF Conference on Computer Vision and Pattern Recognition (CVPR)*, pages 3626–3636, June 2022.
- [49] A Sreekha, Kusum Bashetty, et al. Infinite to finite: an overview of finite element analysis. *Indian Journal of Dental Research*, 21(3):425, 2010.
- [50] Gilbert Strang. On the construction and comparison of difference schemes. *SIAM journal on numerical analysis*, 5(3):506–517, 1968.
- [51] Peter Toth, Danilo J Rezende, Andrew Jaegle, Sébastien Racanière, Aleksandar Botev, and Irina Higgins. Hamiltonian generative networks. In *International Conference on Learning Representations*, 2019.
- [52] Honghui Wang, Yifan Pu, Shiji Song, and Gao Huang. Advancing generalization in pinns through latent-space representations. *IEEE Transactions on Neural Networks and Learning Systems*, 2025.

- [53] Sifan Wang and Paris Perdikaris. Long-time integration of parametric evolution equations with physics-informed deepnets. *Journal of Computational Physics*, 475:111855, 2023.
- [54] Sifan Wang, Shyam Sankaran, and Paris Perdikaris. Respecting causality is all you need for training physics-informed neural networks. *arXiv preprint arXiv:2203.07404*, 2022.
- [55] Sifan Wang, Yujun Teng, and Paris Perdikaris. Understanding and mitigating gradient flow pathologies in physics-informed neural networks. *SIAM Journal on Scientific Computing*, 43(5):A3055–A3081, 2021.
- [56] Sifan Wang, Hanwen Wang, and Paris Perdikaris. Learning the solution operator of parametric partial differential equations with physics-informed deepnets. *Science advances*, 7(40):eabi8605, 2021.
- [57] Sifan Wang, Xinling Yu, and Paris Perdikaris. When and why pinns fail to train: A neural tangent kernel perspective. *Journal of Computational Physics*, 449:110768, 2022.
- [58] Tianshu Wen, Kookjin Lee, and Youngsoo Choi. Reduced-order modeling for parameterized pdes via implicit neural representations. *arXiv preprint arXiv:2311.16410*, 2023.
- [59] Jiachen Yao, Chang Su, Zhongkai Hao, Songming Liu, Hang Su, and Jun Zhu. Multiadam: Parameter-wise scale-invariant optimizer for multiscale training of physics-informed neural networks. In *Proceedings of the 40th International Conference on Machine Learning, ICML’23*. JMLR.org, 2023.
- [60] Yuan Yin, Matthieu Kirchmeyer, Jean-Yves Franceschi, Alain Rakotomamonjy, and Patrick Gallinari. Continuous pde dynamics forecasting with implicit neural representations. *arXiv preprint arXiv:2209.14855*, 2022.
- [61] Bing Yu et al. The deep ritz method: a deep learning-based numerical algorithm for solving variational problems. *Communications in Mathematics and Statistics*, 6(1):1–12, 2018.
- [62] Sihyun Yu, Jihoon Tack, Sangwoo Mo, Hyunsu Kim, Junho Kim, Jung-Woo Ha, and Jinwoo Shin. Generating videos with dynamics-aware

implicit generative adversarial networks. In *International Conference on Learning Representations*, 2022.

Appendix A. Additional Statistical Analysis on CDR Equations

In this section, we provide additional statistical analysis with two other metrics, explained variance score (Exp. var.) and max error (Max. err.), and summarize the results in Table A.2.

Table A.2: The max error and explained variance score over all the equations with the initial condition of Gaussian distribution $N(\pi, (\pi/2)^2)$.

PDE type	Coefficient range	Metric	PINN	PINN-P	P ² INN	DLDMF
Convection	1~5	Max. err. Exp. var.	0.0513 0.9948	0.0601 0.9919	0.2751 0.6070	0.0293 0.9997
	1~10	Max. err. Exp. var.	0.0593 0.9952	0.1681 0.8227	0.3744 0.3009	0.0496 0.9985
	1~20	Max. err. Exp. var.	0.2431 0.6076	0.3173 0.4107	0.4190 0.1500	0.1430 0.9887
Diffusion	1~5	Max. err. Exp. var.	0.3989 -0.1383	0.5190 -1.0922	0.5784 -1.5233	0.4382 -0.4871
	1~10	Max. err. Exp. var.	0.6194 -5.4421	0.7576 -8.4565	0.7638 -7.6938	-0.4871 -2.0589
	1~20	Max. err. Exp. var.	1.3538 -79.3751	1.4417 -85.9107	0.7564 -13.9281	0.4516 -6.3671
Reaction	1~5	Max. err. Exp. var.	0.4053 0.6232	0.4093 0.6123	0.7653 -0.1824	0.0142 0.9999
	1~10	Max. err. Exp. var.	0.7040 0.3008	0.5116 0.5036	0.8847 -0.0936	0.0376 0.9995
	1~20	Max. err. Exp. var.	0.8529 0.1492	0.7022 0.2561	0.9429 -0.0478	0.0846 0.9977
Conv.-Diff.	1~5	Max. err. Exp. var.	0.1412 0.7469	0.1601 0.6008	0.3062 0.2710	0.0399 0.0892
	1~10	Max. err. Exp. var.	0.2171 -0.4752	0.3023 -1.2314	0.3634 -0.3168	0.3169 0.6039
	1~20	Max. err. Exp. var.	0.5396 -19.0867	0.5468 -17.8158	0.3606 -0.4771	0.4549 0.0253
Reac.-Diff.	1~5	Max. err. Exp. var.	0.4901 0.1600	0.5272 -0.2223	0.7646 -0.3109	0.4335 0.5052
	1~10	Max. err. Exp. var.	0.8332 -1.0339	0.7536 -1.0530	0.8982 -0.6734	0.7501 -0.4028
	1~20	Max. err. Exp. var.	0.9637 -1.8660	0.8345 -1.4076	0.9445 -0.5779	1.0133 -3.4065
Conv.-Diff.-Reac.	1~5	Max. err. Exp. var.	0.2694 0.4267	0.3267 0.5533	0.6831 -0.2518	0.2307 0.9333
	1~10	Max. err. Exp. var.	0.6367 0.1239	0.5262 0.3869	0.8418 -0.1386	0.5249 0.7111
	1~20	Max. err. Exp. var.	0.8192 0.0587	0.6859 0.2529	0.9213 -0.0720	0.7230 0.6803

Appendix B. Experiments on Another Initial Condition

In this section, we present the experimental results with the initial condition of $1+\sin(x)$, with other conditions remain unchanged. In Table B.3, we summarize the results in terms of L_2 absolute and relative errors, and in Table ??, we use max error and explained variance score for evaluation. Even with the initial condition of $1+\sin(x)$, our DLDMF shows adequate performance, especially in a wide coefficient range, i.e., 1~20. On top of that, particularly in the case of reaction and conv.-diff.-reac. equations, DLDMF outperforms the baselines by a huge gap.

Table B.3: The relative and absolute L_2 errors over all the equations with the initial condition of $1+\sin(x)$. We do not fine-tune DLD MF for each coefficient setting. However, our pre-trained models already outperform others in many cases.

PDE type	Coefficient range	Metric	PINN	PINN-P	P ² INN	DLD MF
Convection	1~5	Abs. err.	0.0135	0.0073	0.2213	0.0045
		Rel. err.	0.0147	0.0076	0.2159	0.0044
	1~10	Abs. err.	0.0117	0.0233	0.4101	0.0095
		Rel. err.	0.0127	0.0244	0.3821	0.0092
	1~20	Abs. err.	0.1283	0.2558	0.5355	0.0826
		Rel. err.	0.1295	0.2503	0.5092	0.0827
Diffusion	1~5	Abs. err.	0.0496	0.0688	0.2682	0.4027
		Rel. err.	0.0714	0.0956	0.3048	0.4608
	1~10	Abs. err.	0.0835	0.1106	0.3047	0.4863
		Rel. err.	0.1078	0.1416	0.3356	0.5487
	1~20	Abs. err.	0.1206	0.2045	0.3015	0.5254
		Rel. err.	0.1500	0.2333	0.3308	0.5963
Reaction	1~5	Abs. err.	0.2349	0.2396	0.5100	0.0254
		Rel. err.	0.3241	0.3316	0.6117	0.0736
	1~10	Abs. err.	0.5688	0.3418	0.7054	0.0617
		Rel. err.	0.6561	0.4494	0.7994	0.1199
	1~20	Abs. err.	0.7615	0.4290	0.8294	0.1487
		Rel. err.	0.8274	0.5268	0.8987	0.2901
Conv.-Diff.	1~5	Abs. err.	0.0213	0.0182	0.2382	0.1997
		Rel. err.	0.0261	0.0233	0.2605	0.2296
	1~10	Abs. err.	0.0294	0.0345	0.2316	0.1297
		Rel. err.	0.0350	0.0410	0.2574	0.1514
	1~20	Abs. err.	0.0824	0.0960	0.2504	0.1173
		Rel. err.	0.0928	0.1094	0.2741	0.1339
Reac.-Diff.	1~5	Abs. err.	0.0386	0.0368	0.3038	0.1150
		Rel. err.	0.0632	0.0581	0.3562	0.1566
	1~10	Abs. err.	0.2305	0.1632	0.5427	0.0816
		Rel. err.	0.2681	0.2054	0.5807	0.1190
	1~20	Abs. err.	0.5454	0.3107	0.6892	0.0413
		Rel. err.	0.5710	0.3497	0.7131	0.0727
Conv.-Diff.-Reac.	1~5	Abs. err.	0.0593	0.0932	0.3626	0.0551
		Rel. err.	0.0899	0.1465	0.4554	0.0735
	1~10	Abs. err.	0.4953	0.3407	0.6500	0.0337
		Rel. err.	0.5341	0.4006	0.7196	0.0538
	1~20	Abs. err.	0.7329	0.4283	0.8101	0.0614
		Rel. err.	0.7663	0.4911	0.8588	0.1240